UCRL- 96074
PREPRINT

SCATTERING FROM AN OPEN SPHERICAL SHELL HAVING A CIRCULAR APERTURE AND ENCLOSING A CONCENTRIC DIELECTRIC SPHERE

R. W. Ziolkowski, D. P. Marsland,
L. F. Libelo, G. Pisane

This Paper was Prepared for Submittal to
IEEE Transactions on
Antennas & Propagation

February 1987

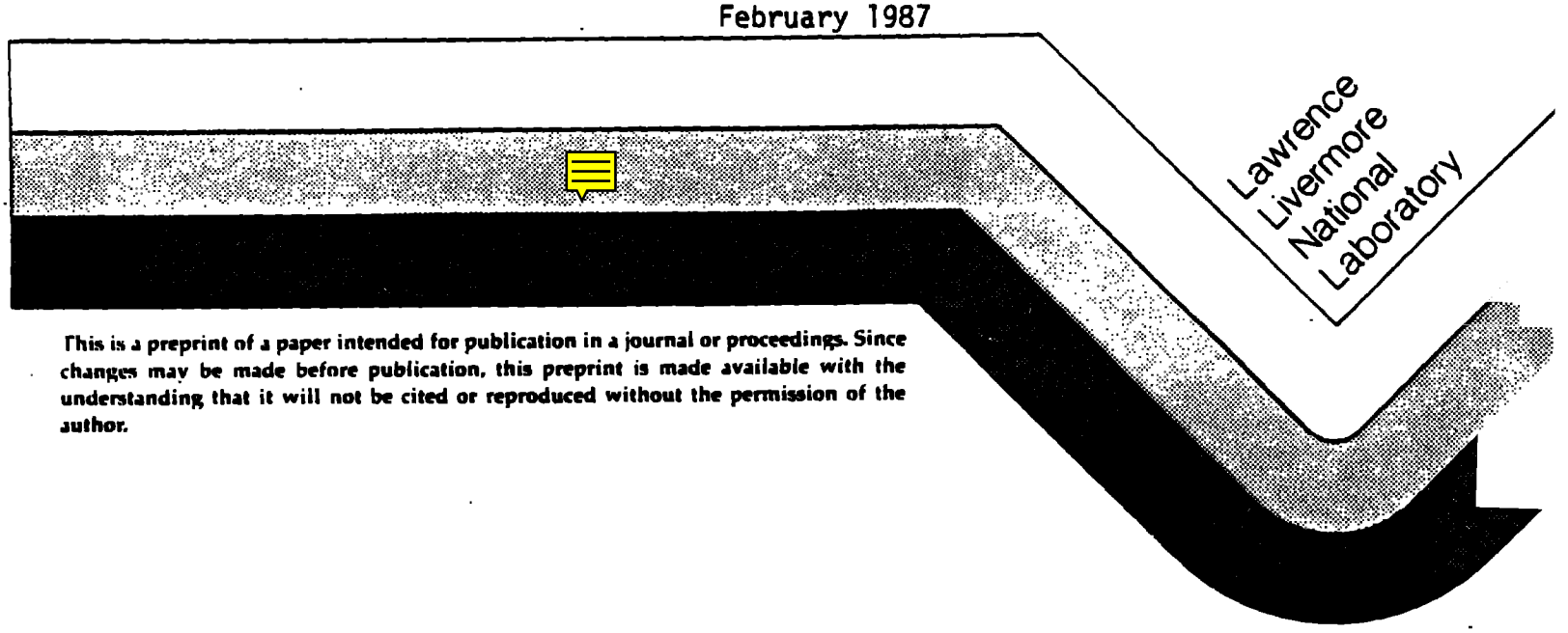

DISCLAIMER

SCATTERING FROM AN OPEN SPHERICAL SHELL HAVING A CIRCULAR APERTURE AND ENCLOSING A CONCENTRIC DIELECTRIC SPHERE

Richard W. Ziolkowski and *Diane P. Marsland*
Engineering Research Division
Lawrence Livermore National Laboratory
P.O. Box 5504, L-156
Livermore, CA 94550

and

Louis F. Libelo and *Guy Pisane*
Harry Diamond Laboratories
2800 Power Mill Road
Adelphi, MD 20783

ABSTRACT

The generalized dual series solution to the scattering of an arbitrary plane wave from an open spherical shell having a circular aperture and enclosing a concentric, homogeneous dielectric sphere is presented. This solution explicitly exhibits the correct edge behavior, and it can handle spheres that are electrically small or large without special considerations. A variety of cross-section results are presented for the normally incident case. It is shown that effects corresponding to the presence of the interior cavity dominate all of the scattering data. In particular, the cross-sections exhibit new resonance features that are due to the cavity-backed nature of the aperture and depend on the characteristics of the interior sphere. The results demonstrate that interior information is contained in the exterior scattering data.

PACS number: 41.10.Hv, 03.80.+r

I. INTRODUCTION

Because they describe coupling via apertures into enclosed regions containing additional dielectric or metallic bodies *and* scattering from reflector structures having edges and nontrivial configurations, the importance of canonical electromagnetic cavity-backed aperture problems can not be understated. They provide a fundamental means with which basic aperture coupling and reflector physics can be studied in detail; they can be used to construct and/or validate approximate models or general engineering analysis and design "rules of thumb" that can be applied to more general apertures and scattering objects; and they aid in the development of improved numerical techniques especially near the edges of the apertures or reflectors where discontinuities appear and where those methods may encounter difficulties. Moreover, accurate canonical solutions of this type provide standards to which general purpose numerical code results can be compared.

A number of canonical problems that describe coupling through apertures into enclosed regions have been solved recently with the generalized dual series (GDS) approach and have been reported elsewhere[1-5]. In two-dimensions these include the scattering of E- and H- polarized plane waves from an empty infinite circular cylinder having an infinite axial slot [1,2] and from one that encloses an infinite concentric [3,4] or off-set impedance cylinder [5]. These two-dimensional slit cylinder problems have proved to be valuable for EMP studies. The locations of field hotspots near the interior object and the current peaks induced on an interior wire are being studied as a function of all of the problem parameters. In three-dimensions the scattering of an arbitrary plane wave from an empty open spherical shell with a circular aperture has been solved [6,7]. These problems have been studied extensively to determine the effects on the aperture coupling and scattering of variations in the polarization, frequency, angle of incidence, aperture size, and interior object characteristics. The GDS solutions are systematic and inherently contain the behavior near the rim of the aperture required by Meixner's edge conditions. They can handle open spheres

that are electrically small or large and arbitrary angles of incidence without additional special considerations. The three-dimensional open spherical shell problems are important because they involve a finite scatterer for which experimental data can be obtained.[8]

In this paper we extend the open spherical shell solution to the case where it encloses a concentric, homogeneous dielectric sphere. Because of length considerations, we will discuss only the normally incident case. As will be described below, these results are readily extended to an incidence angle as described in Ref. 6.

This dual series solutions is the first of its kind for a loaded, open sphere problem. On the other hand, the closed spherical cavity loaded with a concentric, lossy dielectric core has been analyzed for microwave fusion studies.[9-12] Initial heating rates of a plasma core and perturbations of the eigenmodes caused by deformations of the plasma core were investigated. The closed, loaded cavity problem results were recently extended to aid in the explanation of the resonance phenomena to be presented below.[13]

It has been found that resonance features corresponding to the presence of the interior cavity dominate all of the aperture coupling and the scattering results. These include the currents induced on the exterior scatterer, the fields in the aperture, the energy captured by the open cavity, and the scattering cross-sections. As will be demonstrated below, the locations in frequency of these cavity-backed aperture (CBA) resonances and the resultant current and field patterns at those values can be identified with corresponding closed-cavity resonance locations and patterns.

II. DESCRIPTION OF THE PROBLEM

A cross-section of the generic problem configuration is shown in Figure 1. A perfectly conducting, infinitesimally thin, open spherical shell is represented by the surface $\{r = a, 0 \leq \theta < \theta_0\}$ in the spherical coordinate system (r, θ, ϕ) erected at the shell's center. The negative z-axis of that system passes through the center of the aperture, the latter being defined as $\{(r, \theta, \phi) | r = a \text{ and } \theta_0 < \theta \leq \pi\}$. The interior dielectric sphere has a radius

b and a dielectric constant $\epsilon = \epsilon_r \epsilon_0$, where ϵ_0 is the dielectric permittivity of free-space. Half the angular extent of the aperture is measured by the angle $\theta_{ap} = \pi - \theta_0$. The unit vectors $(\hat{r}, \hat{\theta}, \hat{\phi})$ are defined in the standard manner in the directions of positively increasing coordinate values. We divide the problem space into three radial subregions defined by the expressions:

$$\textit{Region I}: \quad \{(r,\theta,\phi)|r > a\}$$

$$\textit{Region II}: \quad \{(r,\theta,\phi)|b < r < a\}$$

$$\textit{Region III}: \quad \{(r,\theta,\phi)|r < b\}.$$

A plane wave

$$\begin{pmatrix} \vec{E}^{inc} \\ \vec{H}^{inc} \end{pmatrix}(r,\theta,\phi) = -E_0\, e^{i\vec{k}\cdot\vec{r}} \begin{pmatrix} \hat{x} \\ Y_0 \cos\theta^{inc}\, \hat{y} \end{pmatrix} \tag{1}$$

is normally incident on the open sphere. Throughout this paper, an $e^{-i\omega t}$ time dependence is assumed and suppressed. The incident angle $\theta^{inc} = 0 \text{ or } \pi$.

Following standard analyses of problems in a spherically symmetric geometry, we employ a Debye potential formalism. In particular, if the radial vector $\vec{r} = r\hat{r}$, the electric and magnetic fields are expressed in terms of the two Hertzian potentials $\Phi\,\vec{r}$ and $\Psi\,\vec{r}$ as

$$\begin{aligned} \vec{E} &= -curl(\Phi\,\vec{r}) - (i\omega\epsilon)^{-1}\, curl\, curl(\Psi\,\vec{r}) \\ \vec{H} &= +curl(\Psi\,\vec{r}) - (i\omega\mu)^{-1}\, curl\, curl(\Phi\,\vec{r}). \end{aligned} \tag{2}$$

The function $\Phi = \sum_{m=0}^{\infty}\sum_{n=m}^{\infty} \Phi_{mn} \sin m\phi$ defines the field TE with respect to r, $\Psi = \sum_{m=0}^{\infty}\sum_{n=m}^{\infty} \Psi_{mn} \cos m\phi$ the field TM with respect to r. The assumption of normal incidence reduces these potentials to a single azimuthal mode for both the incident and the scattered fields:

$$\begin{pmatrix} \Phi^{inc} \\ \Phi^{s} \end{pmatrix}(r,\theta,\phi) = \sum_{n=1}^{\infty} \begin{pmatrix} \Phi_{1n}^{inc} \\ \Phi_{1n}^{s} \end{pmatrix}(r,\theta)\, \sin\phi.$$

$$\begin{pmatrix} \Psi^{inc} \\ \Psi_s \end{pmatrix}(r,\theta,\phi) = \sum_{n=1}^{\infty} \begin{pmatrix} \Psi_{1n}^{inc} \\ \Psi_{1n}^{s} \end{pmatrix}(r,\theta)\, \cos\phi.$$

The actual form of the azimuthal modal coefficients of the scattered field, Φ_1^s and Ψ_1^s, depends upon which region r lies in. Enforcing the electromagnetic boundary conditions:

1. E_{tan}^{tot}, H_{tan}^{tot} must be continuous across $r = b$,
2. E_{tan}^{tot} must be continuous across $r = a$;

we obtain fields from (1) that are summarized by the expressions:

$$\begin{aligned}
E_r &= E_0 \sum_{n=1}^{\infty} \{ i\, n(n+1)\, \tau_{1n}\, \frac{Z_n(kr)}{kr}\, \bar{v}_{1n}(\theta) \}\, \sin\theta \cos\phi \\
E_\theta &= E_0 \sum_{n=1}^{\infty} \Big\{ \sigma_{1n}\, Z_n(kr)\, \bar{v}_{1n}(\theta) - i\, \tau_{1n}\, \frac{[kr\, Z_n(kr)]'}{kr}\, \bar{w}_{1n}(\theta) \Big\} \cos\phi \\
E_\phi &= E_0 \sum_{n=1}^{\infty} \Big\{ \sigma_{1n}\, Z_n(kr)\, \bar{w}_{1n}(\theta) - i\, \tau_{1n}\, \frac{[kr\, Z_n(kr)]'}{kr}\, \bar{v}_{1n}(\theta) \Big\} \sin\phi \\
H_r &= -Y_0\, E_0 \sum_{n=1}^{\infty} \{ i\, n(n+1)\, \sigma_{1n}\, \frac{Z_n(kr)}{kr}\, \bar{v}_{1n}(\theta) \}\, \sin\theta \sin\phi \\
H_\theta &= -Y_0\, E_0 \sum_{n=1}^{\infty} \Big\{ \tau_{1n}\, Z_n(kr)\, \bar{v}_{1n}(\theta) - i\, \sigma_{1n}\, \frac{[kr\, Z_n(kr)]'}{kr}\, \bar{w}_{1n}(\theta) \Big\} \sin\phi \\
H_\phi &= -Y_0\, E_0 \sum_{n=1}^{\infty} \Big\{ \sigma_{1n}\, Z_n(kr)\, \bar{w}_{1n}(\theta) - i\, \sigma_{1n}\, \frac{[kr\, Z_n(kr)]'}{kr}\, \bar{v}_{1n}(\theta) \Big\} \cos\phi\,,
\end{aligned} \tag{3}$$

where the terms $\bar{v}_{mn}(\theta) = m\, P_n^{-m}(\cos\theta) / \sin\theta$ and $\bar{w}_{mn}(\theta) = -\partial_\theta P_n^{-m}(\cos\theta)$, and the notation, for example, $[x j_n(x)]'$, means to take the derivative of the expression in the brackets with respect to x. The function $Z_n(kr)$ is composed of linear combinations of spherical Bessel, $j_n(kr)$; Neumann, $n_n(kr)$; and Hankel (of the first kind), $h_n(kr)$ functions depending on the value of r. In particular, for the *incident field* one has for any r: $Z_n(kr) = j_n(kr)$ and the coefficients

$$\begin{pmatrix} \sigma_{mn}^{inc} \\ \tau_{mn}^{inc} \end{pmatrix} = (-1)^{m+1}\, i^n\, \frac{(2n+1)}{n(n+1)}\, \epsilon_m\, (1 - \delta_{0n}) \begin{pmatrix} \bar{v}_{1n} \\ \bar{w}_{1n} \end{pmatrix} (\theta = \theta^{inc})$$

where $\epsilon_m = 1$ if $m = 0$ and $= 2$ if $m \neq 0$ and Kronecker's delta $\delta_{0n} = 1$ if $n = 0$ and $= 0$ if $n \neq 0$. For *normal incidence* these coefficients explicitly reduce to the values:

$$\begin{pmatrix} \sigma_{1n}^{inc} \\ \tau_{1n}^{inc} \end{pmatrix} (\theta^{inc} = 0) = i^n (2n+1) \begin{pmatrix} +1 \\ -1 \end{pmatrix}$$

$$\begin{pmatrix} \sigma_{1n}^{inc} \\ \tau_{1n}^{inc} \end{pmatrix} (\theta^{inc} = \pi) = -(-i)^n (2n+1) \begin{pmatrix} +1 \\ +1 \end{pmatrix}. \tag{4}$$

With the notation

$$\eta_n^e = \frac{j_n(kb)[k'b\, j_n(k'b)]' - j_n(k'b)[kb\, j_n(kb)]'}{j_n(k'b)[kb\, h_n(kb)]' - h_n(kb)[k'b\, j_n(k'b)]'} \tag{5a}$$

$$\eta_n^h = \frac{j_n(kb)[k'b\, j_n(k'b)]' - \epsilon_r j_n(k'b)[kb\, j_n(kb)]'}{\epsilon_r j_n(k'b)[kb\, h_n(kb)]' - h_n(kb)[k'b\, j_n(k'b)]'}$$

$$\xi_n^e(k\tau) = j_n(k\tau) + \eta_n^e\, h_n(k\tau) \tag{5b}$$

$$\xi_n^h(k\tau) = j_n(k\tau) + \eta_n^h\, h_n(k\tau),$$

$$\zeta_n^e(k'\tau) = \left(\frac{i}{kb}\right) \frac{j_n(k'\tau)}{j_n(k'b)[kb\, h_n(kb)]' - h_n(kb)[k'b\, j_n(k'b)]'} \tag{5c}$$

$$\zeta_n^h(k'\tau) = \left(\frac{i}{kb}\right) \frac{j_n(k'\tau)}{\epsilon_r j_n(k'b)[kb\, h_n(kb)]' - h_n(kb)[k'b\, j_n(k'b)]'}$$

the total field expressions then have the form

$$\begin{pmatrix} \sigma_{1n} \\ \tau_{1n} \end{pmatrix} Z_n(k\tau) = \begin{pmatrix} A_{1n}\, \xi_n^e(ka) \\ B_{1n}\, [ka\, \xi_n^h(ka)]' \end{pmatrix} h_n(k\tau) + \begin{pmatrix} \sigma_{1n}^{inc}\, \xi_n^e(k\tau) \\ \tau_{1n}^{inc}\, \xi_n^h(k\tau) \end{pmatrix} \quad \text{in Region I} \tag{6a}$$

$$\begin{pmatrix}\sigma_{1n}\\ \tau_{1n}\end{pmatrix} Z_n(kr) = \begin{pmatrix}[A_{1n}\, h_n(ka) + \sigma_{1n}^{inc}]\, \xi_n^e(kr)\\ \{B_{1n}\,[ka\, h_n(ka)]' + \tau_{1n}^{inc}\}\, \xi_n^h(kr)\end{pmatrix} \qquad \text{in Region II} \qquad (6b)$$

$$\begin{pmatrix}\sigma_{1n}\\ \tau_{1n}\end{pmatrix} Z_n(k'r) = \begin{pmatrix}[A_{1n}\, h_n(ka) + \sigma_{1n}^{inc}]\, \zeta_n^e(k'r)\\ \{B_{1n}\,[ka\, h_n(ka)]' + \tau_{1n}^{inc}\}\, \zeta_n^h(k'r)\end{pmatrix} \qquad \text{in Region III.} \qquad (6c)$$

It is readily verified by inspection that the resulting electric fields are continuous across $r = a$ and because $\xi_n^{e,h}(kb) = \zeta_n^{e,h}(kb)$, the electric and magnetic fields are continuous across $r = b$. We now proceed as in Ref. 6.

The dual series equations are obtained by enforcing the electromagnetic boundary equations:

$E_{tan}^{tot} = 0$ on the open metallic shell;

H_{tan}^{tot} is continuous over the circular aperture.

With the field expressions (5) and the terms

$$\begin{aligned} f_{1n} &= \sigma_{1n}^{inc}\, \xi_n^e(ka) \\ g_{1n} &= \tau_{1n}^{inc}\, \xi_n^h(ka)\,, \end{aligned} \qquad (7)$$

one obtains

$$ika \sum_{n=1}^{\infty} \{A_{1n}\, \xi_n^e(ka) h_n(ka) - f_{1n}\} P_n^{-1} = \qquad (8a)$$

$$\sin\theta\, \partial_\theta \sum_{n=1}^{\infty} \{B_{1n}\,[ka\, \xi_n^h(ka)]'[ka\, h_n(ka)]' - g_{1n}\} P_n^{-1} \qquad (0 \le \theta < \theta_0)$$

$$\sum_{n=1}^{\infty} A_{1n}\, P_n^{-1} = -ika \sin\theta \partial_\theta \sum_{n=1}^{\infty} B_{1n}\, P_n^{-1} \qquad (\theta_0 < \theta \le \pi) \qquad (8b)$$

$$ika \sin\theta \partial_\theta \sum_{n=1}^{\infty} \{A_{1n}\, \xi_n^e(ka) h_n(ka) - f_{1n}\} P_n^{-1} = \qquad (9a)$$

$$\sum_{n=1}^{\infty} \{B_{1n}\,[ka\, \xi_n^h(ka)]'[ka\, h_n(ka)]' - g_{1n}\} P_n^{-1} \qquad (0 \le \theta < \theta_0)$$

$$\sin\theta \partial_\theta \sum_{n=1}^{\infty} A_{1n}\, P_n^{-1} = -ika \sum_{n=1}^{\infty} B_{1n}\, P_n^{-1} \qquad (\theta_0 < \theta \le \pi)\,. \qquad (9b)$$

These coupled dual series equations differ from those obtained in Ref. 6 only through the presence of the terms proportional to η_n^e and η_n^h. Those terms have the same large n behavior as the "original" ones in Ref. 6. In particular, we can define the functions

$$\chi_n^\phi = [ika(2n+1)\,\xi_n^e(ka)\,h_n(ka)] - 1 \tag{10a}$$

$$\tilde{\chi}_n^\psi = -\left\{1 + \frac{4ika}{2n+1}\,[ka\,\xi_n^h(ka)]'\,[ka\,h_n(ka)]'\right\} \tag{10b}$$

which, as n becomes large, behave as $\lim_{n\to\infty}\chi_n^\phi \sim O(n^{-2})$ and $\lim_{n\to\infty}\tilde{\chi}_n^\psi \sim O(n^{-2})$. Consequently, we can use the normal incidence results of Ref. 6 immediately to obtain a coupled system of infinite linear equations for the unknown modal coefficients. With the truncation procedure introduced in Ref. 6, this system is reduced to a finite, numerically tractable one of the form

$$(-2ika\,L_{1\ell}^e)\bar{\beta}_1 + \frac{A_{1\ell}}{\ell+1/2} + \sum_{n=1}^{N}(\chi_n^\phi\,\Gamma_{1,n\ell}^e)\,\frac{A_{1n}}{n+1/2} = 2ika\sum_{n=1}^{N}\Gamma_{1,n\ell}^e\,f_{1n} \tag{11a}$$

$$(-L_{1\ell}^h)\bar{\beta}_1 + B_{1\ell} + \sum_{n=1}^{N}(\tilde{\chi}_n^\psi\,\Gamma_{1,n\ell}^h)\,B_{1n} = -2ika\sum_{n=1}^{N}\Gamma_{1,n\ell}^h\,\frac{g_{1n}}{n+1/2} \tag{11b}$$

$$[-2ika\,(1-\Lambda_{00}^e)]\,\bar{\beta}_1 + (-2ika\,\Lambda_{00}^e)\,\alpha_1 + \sum_{n=1}^{N}(\chi_n^\phi\,\Lambda_{n0}^e)\,\frac{A_{1n}}{n+1/2} = 2ika\sum_{n=1}^{N}\Lambda_{n0}^e\,f_{1n} \tag{11c}$$

$$[-(1-\Lambda_{00}^h)]\bar{\beta}_1 + [-4(ka)^2\,\Lambda_{00}^h]\alpha_1 + \sum_{n=1}^{N}(\tilde{\chi}_n^\psi\,\Lambda_{n0}^h)\,B_{1n} = -2ika\sum_{n=1}^{N}\Lambda_{n0}^h\,\frac{g_{1n}}{n+1/2}, \tag{11d}$$

where the inversion coefficients are

$$\Lambda_{n\ell}^e = \frac{1}{\pi}\left[\frac{\sin(n-\ell)\theta_0}{n-\ell} + \frac{\sin(n+\ell+1)\theta_0}{n+\ell+1}\right] \tag{12a}$$

$$\Lambda^{h}_{n\ell} = \frac{1}{\pi}\left[\frac{\sin(n-\ell)\theta_0}{n-\ell} - \frac{\sin(n+\ell+1)\theta_0}{n+\ell+1}\right] \tag{12b}$$

so that

$$\Gamma^{e,h}_{1,n\ell} = \frac{\Lambda^{e,h}_{n\ell}\,\Lambda^{e,h}_{00} - \Lambda^{e,h}_{n0}\,\Lambda^{e,h}_{0\ell}}{\Lambda^{e,h}_{00}} \tag{12c}$$

$$L^{e,h}_{1\ell} = -\frac{\Lambda^{e,h}_{0\ell}}{\Lambda^{e,h}_{00}}. \tag{12d}$$

The constants, α_1 and $\tilde{\beta}_1$, are introduced in the solution process to permit a pseudo-decoupling [6,14] of the TE and the TM dual series equations systems and to guarantee satisfaction of Meixner's edge conditions. This system can be solved for the modal coefficients $A_{1\ell}$ and $B_{1\ell}$ with $\ell = 1, 2, \ldots, N$, for instance, by Gauss elimination. Any additional coefficients up to some value L can then be generated recursively from Eqs.(11) by setting $\ell = N+1, N+2, \ldots, L$. Convergence is obtained typically with a value of $N = 10\,ka$ so that $(ka/N)^2$ is small. The following results are derived from Eqs. (11) in this manner. Nonnormal incidence cases are treated in a similar fashion by solving systems analogous to Eqs. 11 for each azimuthal mode and then incorporating the requisite azimuthal mode sums in the desired observables. The associated inversion coefficients analogous to $\Gamma^{e,h}_{1,n\ell}$ and $L^{e,h}_{1\ell}$ are derived in Ref. 6.

III. RESULTS

Any electromagnetic quantity can be calculated once the modal coefficients are determined. In our analysis of the coupling of the plane wave to the dielectrically loaded open sphere, we have stressed the scattering cross-sections (bistatic, radar, forward, and total differential) of this system and the total energy captured by it. The associated formulas for these quantities will be given below before the discussion of the numerical results.

IIIa. REQUISITE FORMULAE

The scattering cross-sections all deal with the far-field behavior of the scattered fields. In particular, the *bistatic cross-section* is given by the expression:

$$\sigma_{BS}(\theta,\phi;\theta^{inc},\phi^{inc}) = \lim_{r\to\infty} 4\pi r^2 \frac{|E^s(r,\theta,\phi)|^2}{|E^{inc}(r,\theta,\phi)|^2}$$

$$= \frac{4\pi}{k^2}\left\{\left|\sum_{n=1}^{\infty}(-1)^n\left[\sigma_{1n}^I\bar{v}_{1n}(\theta)+\tau_{1n}^I\bar{w}_{1n}(\theta)\right]\right|^2\cos^2\phi\right.$$

$$\left.+\left|\sum_{n=1}^{\infty}(-1)^n\left[\sigma_{1n}^I\bar{w}_{1n}(\theta)+\tau_{1n}^I\bar{v}_{1n}(\theta)\right]\right|^2\sin^2\phi\right\} \qquad (13)$$

which for $\theta = \theta^{inc}+\pi$ and $\phi = 0°$ gives the radar cross-section:

$$\sigma_{RCS} = \sigma_{BS}(\theta^{inc}+\pi,0;\theta^{inc},\phi^{inc}) = \frac{\pi}{k^2}\left|\sum_{n=-\infty}^{\infty} i^n\left[\sigma_{1n}^I+\tau_{1n}^I\right]\right|^2 \qquad (14)$$

which for $\theta = \theta^{inc}$ and $\phi = 0°$ gives the *forward cross-section*:

$$\sigma_{FCS} = \sigma_{BS}(\theta^{inc},0;\theta^{inc},\phi^{inc}) = \frac{\pi}{k^2}\left|\sum_{n=-\infty}^{\infty}(-i)^n\left[\sigma_{1n}^I-\tau_{1n}^I\right]\right|^2, \qquad (15)$$

where from (6a) the scattered field coefficients for $r > a$ are defined as

$$\sigma_{1n}^I = A_{1n}\,\xi_n^e(ka)+\eta_n^e\,\sigma_{1n}^{inc} \qquad (16a)$$

$$\tau_{1n}^I = B_{1n}\left[ka\xi_n^h(ka)\right]'+\eta_n^h\,\tau_{1n}^{inc}\,. \qquad (16b)$$

These cross-sections indicate the amount of field scattered in particular directions. To make a connection of these formulas with the standard ones for the closed sphere, notice

that in the limit $\theta_0 \to \pi$, where the shell is closed, the empty sphere solution coefficients reduce to the forms[6]

$$A_{1n}(\theta_0 = pi) = -\frac{i^n\,(2n+1)}{h_n(ka)} = (2n+1)\,\frac{a_n}{j_n(ka)}$$

$$B_{1n}(\theta_0 = pi) = \frac{i^n\,(2n+1)}{[ka\,h_n(ka)]'} = -(2n+1)\,\frac{b_n}{[ka\,j_n(ka)]'}\,.$$

Consequently, the standard closed sphere radar cross-section result is, for instance, recovered:

$$\sigma_{RCS}^{closed} = \frac{\pi}{k^2}\left|\sum_{n=1}^{\infty}(-1)^{n+1}\,(2n+1)\,(a_n - b_n)\right|^2. \tag{17}$$

In contrast, the *total differential or scattering cross-section*:

$$\sigma_{tot} = \lim_{r\to\infty}\frac{\frac{1}{2}\int \mathrm{Re}\left[(\vec{E}_s \times \vec{H}_s^*)\cdot\hat{r}\right] r^2\,\sin\theta\,d\theta d\phi}{\frac{1}{2}\,Y_0\,|E_0|^2}$$

$$= \frac{2\pi}{k^2}\sum_{n=1}^{\infty}\frac{[|\sigma_{1n}^{>}|^2 + |\tau_{1n}^{>}|^2]}{2n+1} \tag{18}$$

is representative of the energy scattered into the entire 4π-sphere.

The total energy captured by the open scattering object is an important measure of the amount of coupling the incident field experiences through the aperture into the object's interior. The total energy captured in the dielectrically loaded open sphere is given by the complicated expression

$$U_{tot} = \frac{1}{2}\int_0^b\int_0^{\pi}\int_0^{2\pi}\left[|\vec{E}^{III}|^2 + |Z_0\,\vec{H}^{III}|^2\right] r^2\,\sin\theta\,dr d\theta d\phi$$
$$+\frac{1}{2}\int_b^a\int_0^{\pi}\int_0^{2\pi}\left[|\vec{E}^{II}|^2 + |Z_0\,\vec{H}^{II}|^2\right] r^2\,\sin\theta\,dr d\theta d\phi$$

$$= 2\pi E_0^2\, b^3 \sum_{n=1}^{\infty}(2n+1)|u_n^{III}|^2\left[j_n^2(k'b) - j_{n-1}(k'b)j_{n+1}(k'b)\right]$$

$$+2\pi E_0^2 \sum_{n=1}^{\infty}(2n+1)\Big[|u_{1n}^{II}|^2\Big\{a^3[j_n^2(ka)-j_{n-1}(ka)j_{n+1}(ka)]-b^3[j_n^2(kb)-j_{n-1}(kb)j_{n+1}(kb)]\Big\}$$

$$+|u_{2n}^{II}|^2\left\{a^3[j_n(ka)n_n(ka) - \frac{1}{2}\{j_{n+1}(ka)n_{n-1}(ka) + j_{n-1}(ka)n_{n+1}(ka)]\}\right.$$

$$\left. - b^3[j_n(kb)n_n(kb) - \frac{1}{2}\{j_{n+1}(kb)n_{n-1}(kb) + j_{n-1}(kb)n_{n+1}(kb)]\right\}$$

$$+|u_{3n}^{II}|^2\left\{a^3[n_n^2(ka) - n_{n-1}(ka)n_{n+1}(ka)] - b^3[n_n^2(kb) - n_{n-1}(kb)n_{n+1}(kb)]\right\}\Big] \qquad (19)$$

where the following notation has been introduced

$$|u_n^{III}|^2 = \frac{|\sigma_{1n}^{III}|^2 + |\tau_{1n}^{III}|^2}{(2n+1)^2} \qquad (20a)$$

$$|u_{1n}^{II}|^2 = \frac{|\sigma_{1n}^{II}|^2\,(1 + 2\eta_e^r + |\eta_e|^2) + |\tau_{1n}^{III}|^2\,(1 + 2\eta_h^r + |\eta_h|^2)}{(2n+1)^2} \qquad (20b)$$

$$|u_{2n}^{II}|^2 = \frac{|\sigma_{1n}^{II}|^2\,(2\eta_e^r) + |\tau_{1n}^{III}|^2\,(2\eta_h^i)}{(2n+1)^2} \qquad (20c)$$

$$|u_{3n}^{II}|^2 = \frac{|\sigma_{1n}^{II}|^2\,|\eta_e|^2 + |\tau_{1n}^{III}|^2\,|\eta_h|^2}{(2n+1)^2} \qquad (20d)$$

and from Eqs. (6b) and (6c) the coefficients

$$\sigma_{1n}^{II} = A_{1n}\,h_n(ka) + \sigma_{1n}^{inc} \qquad (21a)$$

$$\tau_{1n}^{II} = B_{1n}\,[ka\,h_n(ka)]' + \tau_{1n}^{inc} \qquad (21b)$$

$$\sigma_{1n}^{III} = \frac{i}{kb}\,\frac{A_{1n}\,h_n(ka) + \sigma_{1n}^{inc}}{j_n(k'b)[kb\,h_n(kb)]' - h_n(kb)[k'b\,j_n(k'b)]'} \qquad (21c)$$

$$\tau_{1n}^{III} = \frac{i}{kb}\,\frac{B_{1n}\,[ka\,h_n(ka)]' + \tau_{1n}^{inc}}{\epsilon_r j_n(k'b)[kb\,h_n(kb)]' - h_n(kb)[k'b\,j_n(k'b)]'}\,. \qquad (21d)$$

The results for the total energy will be presented as a figure of merit defined by the ratio: U_{tot}/U_{inc}, of the total field energy in the dielectrically loaded open sphere to the incident field energy in the corresponding dielectrically loaded mathematical sphere with $r \leq a$:

$$U_{inc} = 2\pi E_0^2 \sum_{n=1}^{\infty}(2n+1)|u_n^{inc}|^2\Big\{b^3\left[j_n^2(k'b) - j_{n-1}(k'b)j_{n+1}(k'b)\right] + a^3\left[j_n^2(ka) - j_{n-1}(ka)j_{n+1}(ka)\right] - b^3\left[j_n^2(kb) - j_{n-1}(kb)j_{n+1}(kb)\right]\Big\} \qquad (22a)$$

where the coefficients

$$|u_n^{inc}|^2 = \frac{|\sigma_{1n}^{inc}|^2 + |\tau_{1n}^{inc}|^2}{(2n+1)^2}. \qquad (22b)$$

IIIb. NUMERICAL RESULTS

The dominance of the resonance features, corresponding to the presence of the interior cavity, in all of the aperture coupling and scattering results is first illustrated in Fig. 2. Included are the radar (Fig. 2a) and forward (Fig. 2b) cross-sections normalized to πa^2, the aperture field $E_\theta^s(a,\pi,0)$ (Fig. 2c), and the energy density ratio U_{tot}/U_{inc} (Fig. 2d) for a unit amplitude plane wave incident at $\theta = 0°$ upon an open sphere with $\theta_{ap} = 10°$ and radius a enclosing a dielectric sphere of radius $b = 0.3a$ and relative permittivity $\epsilon_r = 3.0$. The peaks of the anti-resonance features in the radar cross-section occur at $ka =$ 2.5825, 3.822, 4.271, 4.939, and 5.326, and correspond to the TM_{11}, TM_{21}, TE_{11}, TM_{31}, and TM_{12} modes. The corresponding valleys occur at $ka = 2.5827$, 3.823, 4.272, 4.945, and 5.328. These mode assignments were made by tracking the resonance locations from the corresponding closed sphere to the present open sphere cases.[13]

As discussed in Ref.15, the open sphere results are closely correlated with the closed sphere results at lower ka values except for the presence of the CBA resonance features. As ka increases (wavelength decreases) so that the incident wave can begin to sense the

presence of the aperture and the interior cavity, the deviation of the open sphere from the closed sphere results increases. This effect is clearly perceived in Fig. 2c where for the closed sphere case the scattered field would have a unit amplitude at $(a, \pi, 0)$. The peaks in the resonance locations in Fig. 2d occur at ka = 2.5825, 3.822, 4.271, 4.942, and 5.327. These are slightly lower in ka than the corresponding closed cavity values: 2.5854, 3.833, 4.275, 4.966, and 5.332. This effect is due to the detuning of the cavity by the aperture.

The difference in locations of the peaks of σ_{RCS} and U_{tot}/U_{inc} is characteristic of a CBA configuration. In particular, consider Fig. 3 where the TM_{21} resonance region of Figs. 2a and 2d are superimposed. As discussed in Ref. 15, the resonance peaks are indicative of a reradiation phenomenon that is associated with the cavity-backed nature of the aperture. As indicated by Fig. 3, the energy contained within the open spherical shell dramatically increases at a CBA resonance. Concurrently, the currents induced on the sphere and (as a consequence) the scattered fields experience a π-phase shift as ka passes through one of these CBA resonances. Thus a scattered field, whose amplitude is enhanced by the energy resonantly captured in the cavity, is created that at different look angles either constructively or destructively interferes with the incident field. As the cavity begins to capture more energy, the radar return increases; while just after resonance the radar return is dramatically smaller and the captured energy begins to decrease. The radar returns then approach their closed sphere values as the stored energy decreases further. This results in the distinctive anti-resonance features present in the radar cross-section.

These resonance features are also found in the bistatic cross-sections at the same relative positions for all look angles. This is demonstrated in Fig. 4 where the E-plane bistatic cross-section of the case in Fig. 2 is given for the look-angles θ = 180° , 135° , 90° , and 45° as functions of ka. As one might expect, the shapes and sizes of the cross-sections as well as the individual resonance peaks vary with the angle of incidence and the bistatic look angles. This behavior is further evidenced in Fig. 5 where the E-plane bistatic cross-sections is given as a function of the bistatic angle θ for ka = 3.8170 (Fig. 5a), 3.8220 (Fig.

5b), 3.8230 (Fig. 5c), and 3.8280 (Fig. 5d). Figs. 5b and 5c correspond, respectively, to the locations very near the peak and the minimum of the associated CBA anti-resonance feature present in Fig. 2a. Comparing Figs. 5a-5d one finds that the enhanced response in the back-scattered direction just before the peak of the resonance occurs at the expense of the signals scattered into the other look angles, particularly in the broadside direction. Similarly, the broadside response is enhanced at the expense of the back-scattered signal just past the anti-resonance minimum.

The fact that the resonance features are very narrow in Fig. 2 is indicative of the extremely high Q nature of the cavity. Increasing the aperture size broadens them, and their locations are translated to lower ka values corresponding to an increased detuning of the cavity. This is illustrated in Fig. 6 where the total differential cross-sections for a unit amplitude plane wave with $\theta^{inc} = 0°$ is incident on open spheres of radius a with aperture angles $\theta_{ap} = 10°$ (Fig. 6a), 15 ° (Fig. 6b), 20 ° (Fig. 6c), and 30 ° (Fig. 6d), enclosing a dielectric sphere of radius $b = 0.3a$ and relative permittivity $\epsilon_r = 3.0$. The corresponding radar cross-sections are given in Figs. 7a-7d. The movement of the RCS peaks and valleys are readily traced as the aperture size increases.

The locations of the CBA resonances are also dependent on the characteristics of the interior load. This is demonstrated in Figs. 8 and 10. In Fig. 8 a unit amplitude plane wave with $\theta^{inc} = 0°$ is incident on open spheres each with radius a and an aperture angle $\theta_{ap} = 10°$ and enclosing dielectric spheres of relative permittivity $\epsilon_r = 3.0$ and radii $b = 0.1a$ (Fig. 8a), $b = 0.3a$ (Fig. 8b), $b = 0.5a$ (Fig. 8c), $b = 0.8a$ (Fig. 8d). In Fig. 9 a unit amplitude plane wave with $\theta^{inc} = 0°$ is incident on open spheres each with a radius a and an aperture angle $\theta_{ap} = 10°$ and enclosing dielectric spheres of radii $b = 0.3a$ and relative permittivities $\epsilon_r = 1.0$(Fig. 9a), $\epsilon_r = 3.0$ (Fig. 9b), and $\epsilon_r = 10.0$ (Fig. 9c).

As observed in Figs. 8 and 9, there are clear distinctions between all of the cases depending on the properties of the interior dielectric sphere. Some of the resonance locations are nearly coincident while others are not. This depends intimately on the particular

modal pattern that is established in the interior of the cavity. If the mode "interacts" with the interior object, large shifts in the positions of the resonance features may be produced. Comparing the empty and the loaded cavity cases, one finds that as the size of the interior load is increased, very large translations of particular CBA resonance locations occur. As shown, one may observe the sequence in which resonances appear to be altered or even a disappearance of some or the appearance of additional resonances in a fixed ka interval. As the relative permittivity of the interior dielectric sphere is increased, the number of resonances found at lower ka values is dramatically increased. Of course, the number of available cavity modes (hence, CBA resonance features) becomes quite large as ka (frequency) increases.

This behavior of the resonances is explained by analyzing the migration of their locations in the closed cavity case[13] and is illustrated in Figs. 10 and 11. The locations of the resonances are tracked for the corresponding closed metal exterior – $\epsilon_r = 3.0$ interior dielectric sphere case of Fig. 8 as a function of ka and the ratio b/a. As these figures indicate, there is a large variety of structures present in the mode spectrum for the closed cavity. This accounts for the different number of resonances in Figs. 8a-8d for the cavity-backed aperture case and for the difference in their locations. The combination of knowing the location of the closed structure resonances and their anticipated presence in the exterior scattering data has strong implications towards a potential object identification system and is currently being pursued.

IV. DISCUSSION

Parameter studies of the generalized dual series solutions of several cavity-backed aperture canonical problems are enhancing our understanding of the aperture coupling and scattering processes. As shown here for the dielectrically loaded open sphere, the presence of the resonance features in the scattering cross-sections are extremely interesting.

The cross-section resonances indicate that *for cavity-backed apertures there is interior information contained in the exterior scattering data.* The dependence of the location of these peaks on the interior structure and their presence at all look angles may have very important ramifications for diagnostic and object identification applications.

The anti-resonance peaks in the empty open spherical shell and open cylinder radar cross-sections have actually been observed experimentally [9,10]. Nonetheless, for a lack of theoretical proof of their existence, they have been generally attributed to errors in the measurement apparatus.[10] The current analysis is but one attempt to overcome this situation and to make applied physicists as well as engineers aware of the new richness in studying cavity-backed aperture configurations.

ACKNOWLEDGMENTS

This work was performed in part under the auspices of the U. S. Department of Energy by the Lawrence Livermore National Laboratory under contract W-7405-ENG-48 and by Harry Diamond Laboratories.

REFERENCES

[1] R. W. Ziolkowski, SIAM J. Math. Anal., **16**(2), 358 (1985).

[2] W. A. Johnson and R. W. Ziolkowski, Radio Science, **19**(1), 275 (1984).

[3] R. W. Ziolkowski , W. A. Johnson, and K. F. Casey, Radio Sci., **19**(11), 1425 (1984).

[4] R. W. Ziolkowski and J. B. Grant, "Scattering from cavity-backed apertures: The generalized dual series solution of the concentrically loaded E-pol slit cylinder problem", to appear in IEEE Trans. Antennas Prop., 1987.

[5] R. W. Ziolkowski and R. F. Schmucker, "Scattering from a slit cylinder enclosing an off-set impedance surface", Proc. National Radio Science Meeting, U.R.S.I. B8-8, Boulder, CO, Jan. 1986.

[6] R. W. Ziolkowski and W. A. Johnson, "Electromagnetic Scattering of an Arbitrary Plane Wave from a Spherical Shell with a Circular Aperture", to appear in J. Math. Phys., 1987.

[7] R. W. Ziolkowski, "Scattering from a spherical shell with a circular aperture: cross-sections and energy storage for a normally incident plane wave", Proc. National Radio Science Meeting, U.R.S.I. IRC-6, Vancouver, B. C., June 1985.

[8] S. Chang and T. B. A. Senior, "Scattering by a Spherical Shell with a Circular Aperture", AFWL Interaction Notes, Note 141, Apr. 1969.

[9] E. Garelis, Phys. Fluids 17(11), 2002 (1974).

[10] A. D. Steiger, J. Math. Phys. 18(2), 312 (1977).

[11] C. H. Woods, Phys. Fluids 20(2), 252 (1977).

[12] D. L. Ensley, Phys. Fluids 22(12), 2359 (1979).

[13] L. F. Libelo, G. E. Pisane, and R. W. Ziolkowski, Proc. Nuclear EMP Meeting, 104-7.6, Albuquerque, N. M., May, 1986.

[14] R. W. Ziolkowski and W. A. Johnson, "Pseudo-decoupling Ansatz for Electromagnetic Aperture Coupling", to appear in Radio Science, 1987.

[15] R. W. Ziolkowski, "New Electromagnetic Resonance Effects Associated With Cavity-Backed Apertures", to appear in Radio Science, 1987.

LIST OF FIGURES

1. The generic configuration of the scattering of a plane wave from a cavity-backed aperture with an interior dielectric load is depicted.
2. Interior information is present in all of the exterior scattering data. This is demonstrated with ka scans of the (a) radar cross-section, (b) forward cross-section, (c) magnitude of E_θ at the center of the aperture, and (d) the energy density ratio U_{tot}/U_{inc} for a plane wave normally incident into a 10° aperture of an open spherical shell of radius a enclosing a concentric dielectric of radius $b = 0.3a$ and relative permittivity $\epsilon_r = 3.0$.
3. A superimposed, enhanced rendering of the TM_{21} resonance regions of Figs. 2a and 2d elucidates the reradiation behavior of the cavity-backed aperture system.
4. The CBA resonances are present at all bistatic look-angles. This is illustrated with the E-plane bistatic cross-section as a function of ka for a plane wave normally incident into a 10° aperture of an open spherical shell of radius a enclosing a concentric $\epsilon_r = 3.0$ dielectric sphere of radius $b = 0.3a$. The observation angle θ = (a) 180.0° , (b) 135.0° , (c) 90.0° , and (d) 45.0° .
5. More complete views of the bistatic cross-section as a function of the observation angle θ are given for the TM_{21} resonance region of Fig. 4. The ka values are (a) 3.8170, (b) 3.8220, (c) 3.8230, and (d) 3.8280.
6. As the aperture size increases, the cavity becomes more detuned and the resonance features broaden and shift to lower ka. This is illustrated with the total differential cross-sections for a plane wave normally incident into open spherical shells of radius a with (a) 10° , (b) 15° , (c) 20° , and 30° apertures and enclosing a concentric $\epsilon_r = 3.0$ dielectric sphere of radius $b = 0.3a$.
7. The dual series solution allows one to track the movement of the CBA resonances as the aperture size increases. This is illustrated with the radar cross-sections for a plane wave normally incident into open spherical shells of radius a with (a) 10° , (b) 15° , (c)

20° , and 30° apertures and enclosing a concentric $\epsilon_r = 3.0$ dielectric sphere of radius $b = 0.3a$.

8. Interior information is contained in the exterior scattering data. This is shown with the radar cross-sections for a plane wave normally incident into open spherical shells of radius a with a 10° , aperture and enclosing concentric $\epsilon_r = 3.0$ dielectric spheres with radii (a) $b = 0.1a$, (b) $b = 0.3a$, (c) $b = 0.5a$, and $b = 0.8a$.

9. The presence of interior information in the exterior scattering data is also illustrated with the radar cross-sections for a plane wave normally incident into open spherical shells of radius a with a 10° , aperture and enclosing concentric dielectric spheres with radius $b = 0.3a$ and relative permittivities (a) $\epsilon_r = 1.0$, (b) $\epsilon_r = 3.0$, and (c)$\epsilon_r = 10.0$.

10. The behavior of the CBA resonance locations can be predicted by studying the migration of the eigenvalues in the corresponding closed exterior sphere cases. A composite of the trajectories of several TE eigenvalues is given for a spherical cavity of radius a internally loaded with a concentric dielectric sphere of radius b and relative permittivity $\epsilon_r = 3.0$ as the ratio b/a increases versus ka.

11. A composite of the corresponding trajectories of several TM eigenvalues is given for a spherical cavity of radius a internally loaded with a concentric dielectric sphere of radius b and relative permittivity $\epsilon_r = 3.0$ as the ratio b/a increases versus ka.

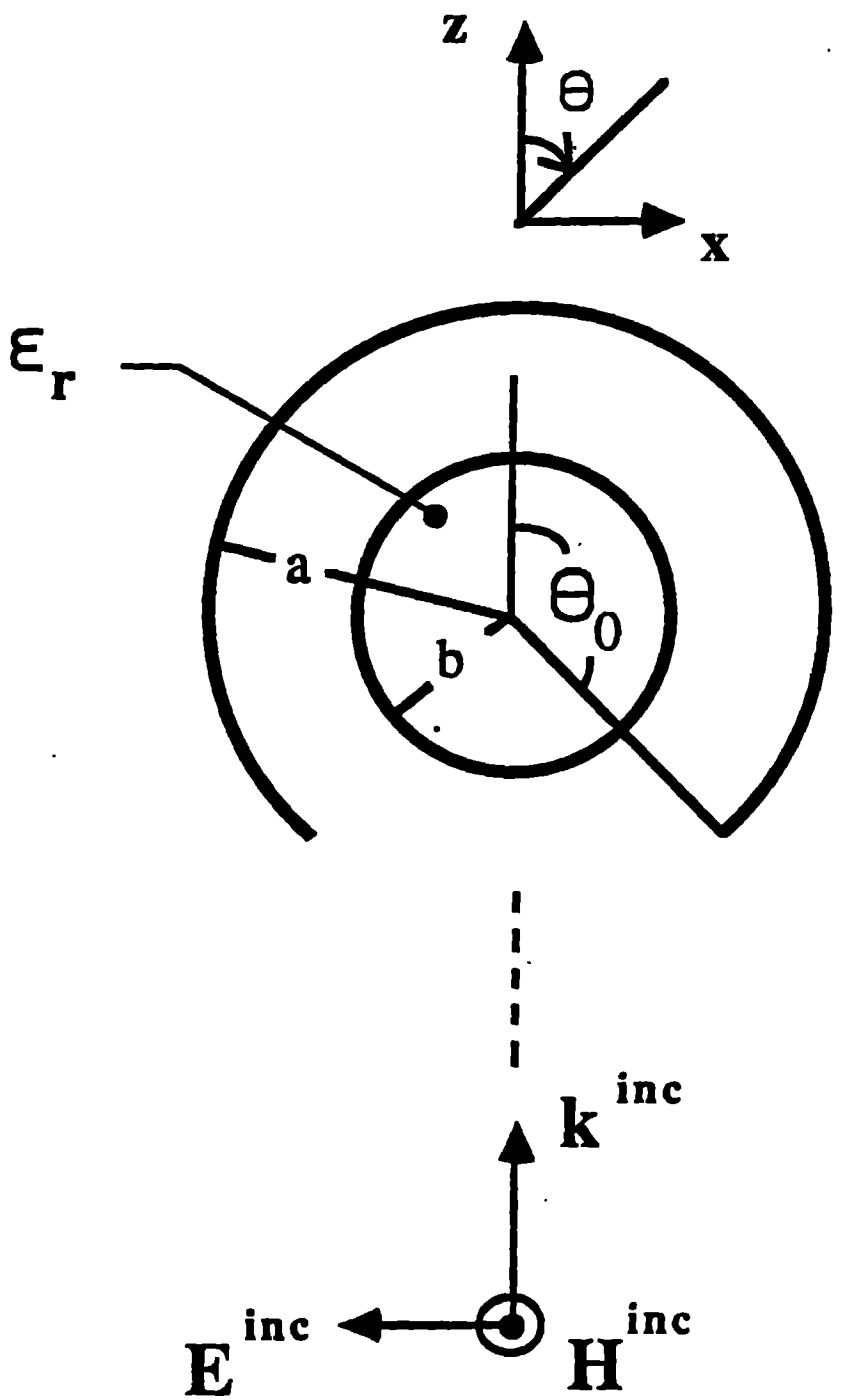

FIGURE 1.

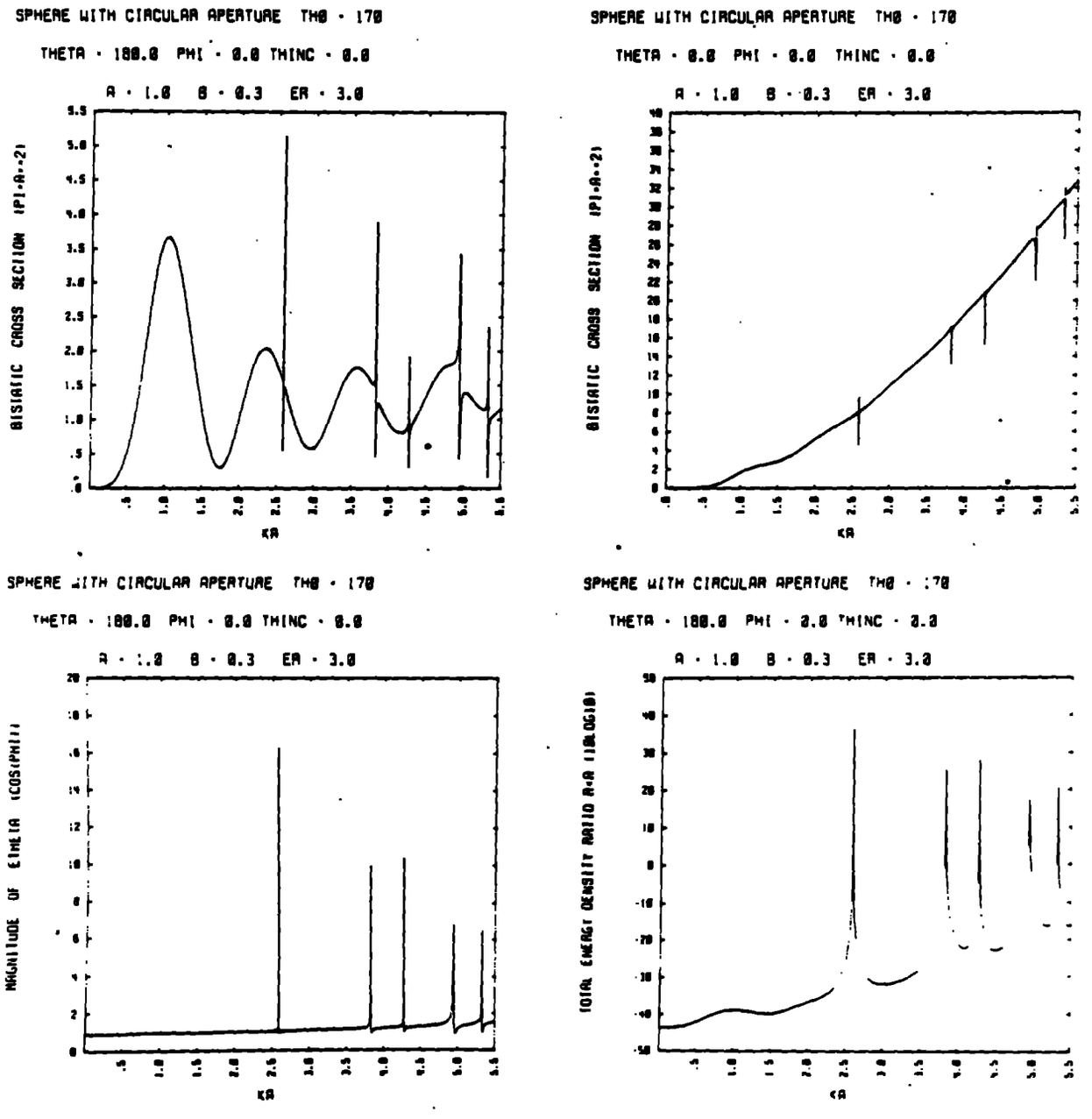
SPHERE WITH CIRCULAR APERTURE THΘ = 17Θ
THETA = 18Θ.Θ PHI = Θ.Θ THINC = Θ.Θ
A = 1.Θ B = Θ.3 ER = 3.Θ
BISTATIC CROSS SECTION (PI-A-2)
KA
SPHERE WITH CIRCULAR APERTURE THΘ = 17Θ
THETA = Θ.Θ PHI = Θ.Θ THINC = Θ.Θ
A = 1.Θ B = Θ.3 ER = 3.Θ
BISTATIC CROSS SECTION (PI-A-2)
KA
SPHERE WITH CIRCULAR APERTURE THΘ = 17Θ
THETA = 18Θ.Θ PHI = Θ.Θ THINC = Θ.Θ
A = 1.Θ B = Θ.3 ER = 3.Θ
KA
SPHERE WITH CIRCULAR APERTURE THΘ = 17Θ
THETA = 18Θ.Θ PHI = Θ.Θ THINC = Θ.Θ
A = 1.Θ B = Θ.3 ER = 3.Θ
KA

Figure 2.

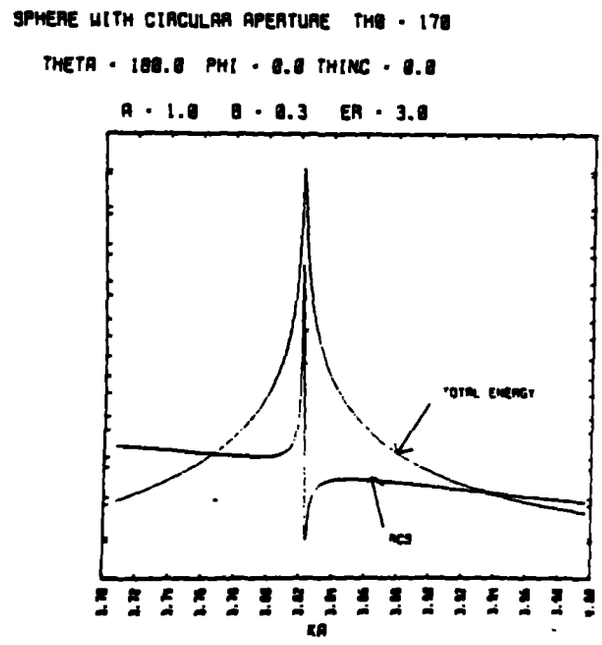
SPHERE WITH CIRCULAR APERTURE THO = 170
THETA = 180.0 PHI = 0.0 THINC = 0.0
A = 1.0 B = 0.3 ER = 3.0
TOTAL ENERGY
RCS
KA

Figure 3.

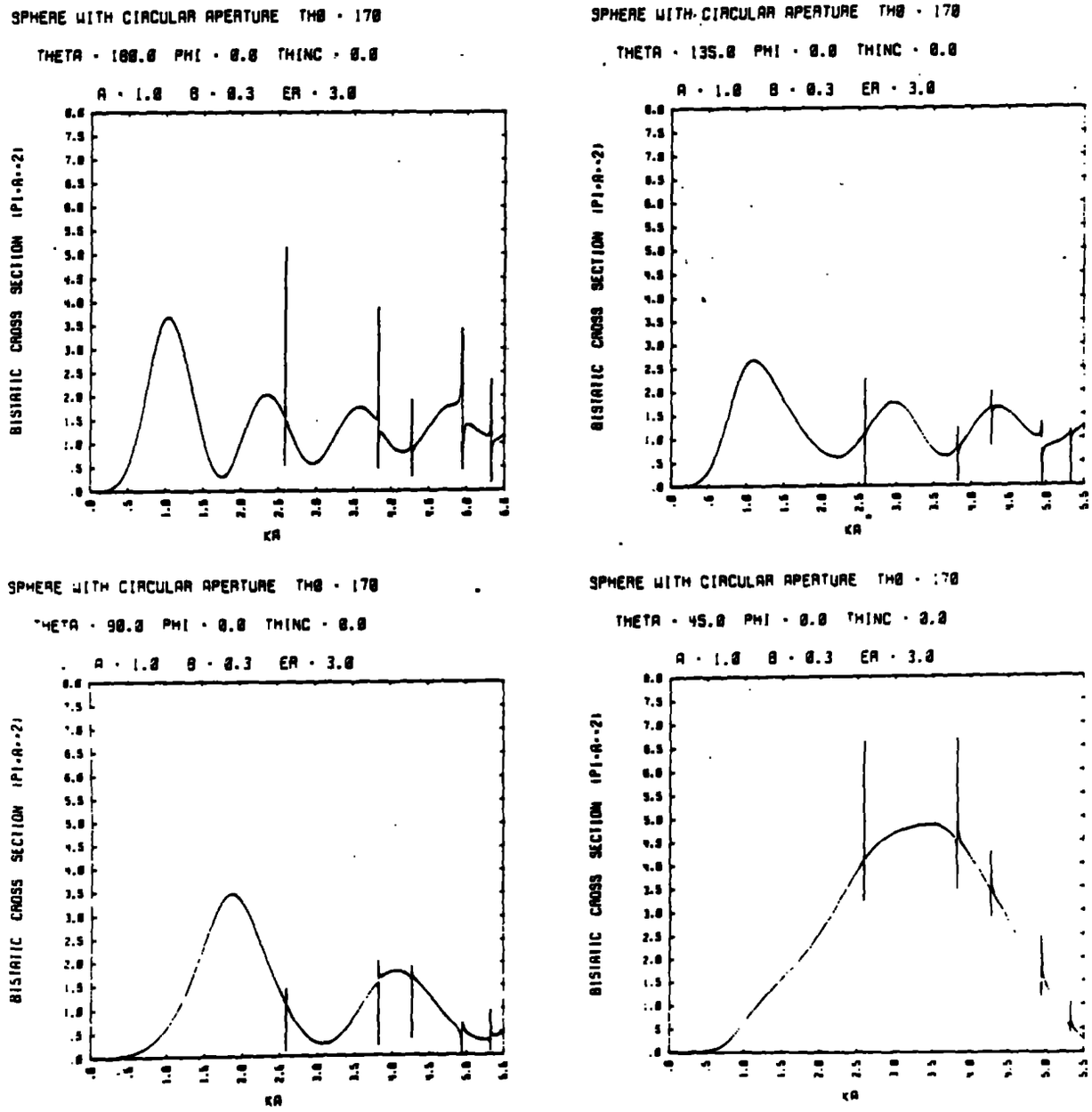
SPHERE WITH CIRCULAR APERTURE TH0 = 170
THETA = 180.0 PHI = 0.0 THINC = 0.0
A = 1.0 B = 0.3 ER = 3.0
BISTATIC CROSS SECTION (PI*A**2)
KA
SPHERE WITH CIRCULAR APERTURE TH0 = 170
THETA = 135.0 PHI = 0.0 THINC = 0.0
A = 1.0 B = 0.3 ER = 3.0
BISTATIC CROSS SECTION (PI*A**2)
KA
SPHERE WITH CIRCULAR APERTURE TH0 = 170
THETA = 90.0 PHI = 0.0 THINC = 0.0
A = 1.0 B = 0.3 ER = 3.0
BISTATIC CROSS SECTION (PI*A**2)
KA
SPHERE WITH CIRCULAR APERTURE TH0 = 170
THETA = 45.0 PHI = 0.0 THINC = 0.0
A = 1.0 B = 0.3 ER = 3.0
BISTATIC CROSS SECTION (PI*A**2)
KA

Figure 4.

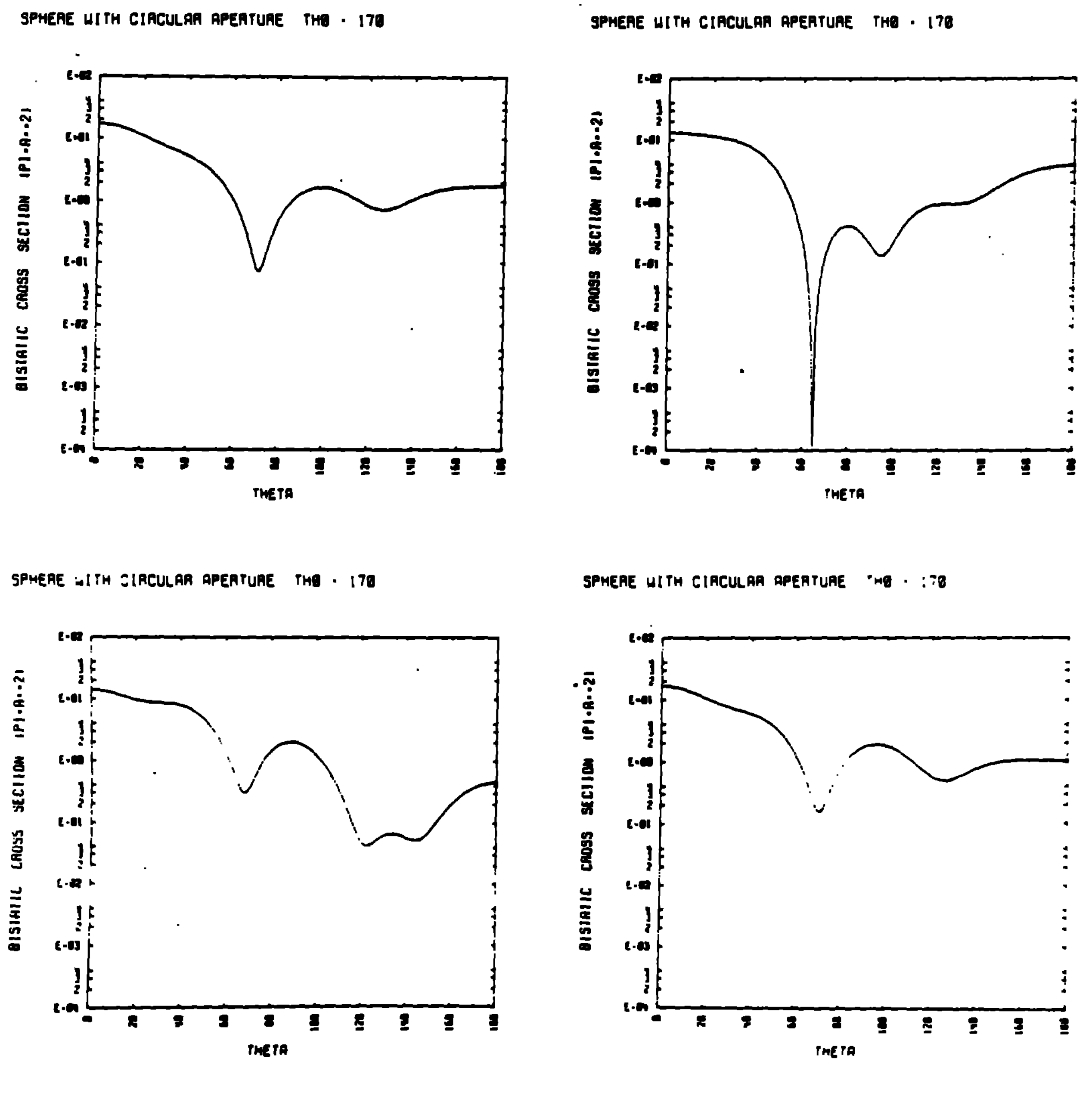
SPHERE WITH CIRCULAR APERTURE TH0 = 170
BISTATIC CROSS SECTION (PI*A**2)
THETA
SPHERE WITH CIRCULAR APERTURE TH0 = 170
BISTATIC CROSS SECTION (PI*A**2)
THETA
SPHERE WITH CIRCULAR APERTURE TH0 = 170
BISTATIC CROSS SECTION (PI*A**2)
THETA
SPHERE WITH CIRCULAR APERTURE TH0 = 170
BISTATIC CROSS SECTION (PI*A**2)
THETA

Figure 5.

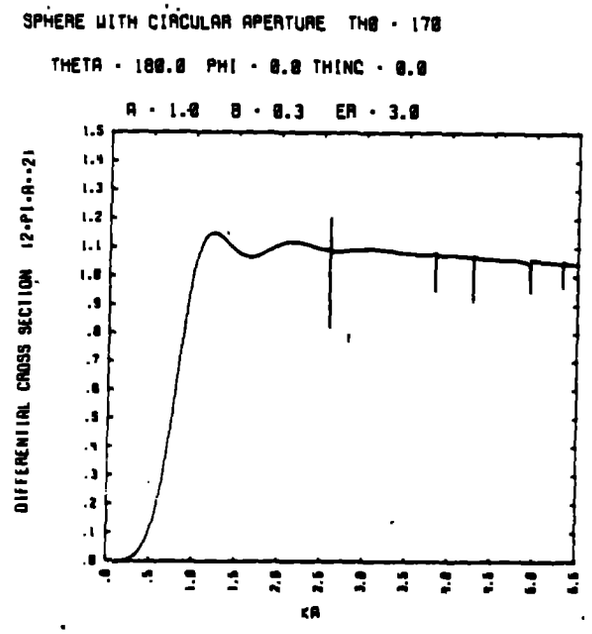
SPHERE WITH CIRCULAR APERTURE TH0 = 170
THETA = 180.0 PHI = 0.0 THINC = 0.0
A = 1.0 B = 0.3 ER = 3.0
DIFFERENTIAL CROSS SECTION (2*PI*A**2)
KA

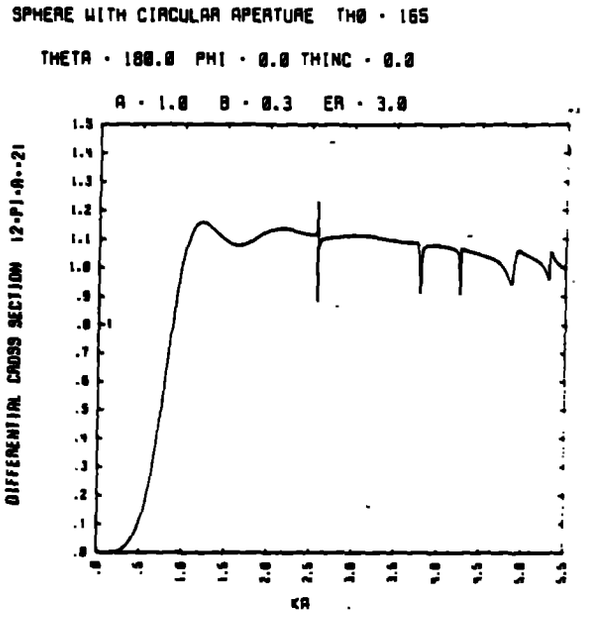
SPHERE WITH CIRCULAR APERTURE TH0 = 165
THETA = 180.0 PHI = 0.0 THINC = 0.0
A = 1.0 B = 0.3 ER = 3.0
DIFFERENTIAL CROSS SECTION (2*PI*A**2)
KA

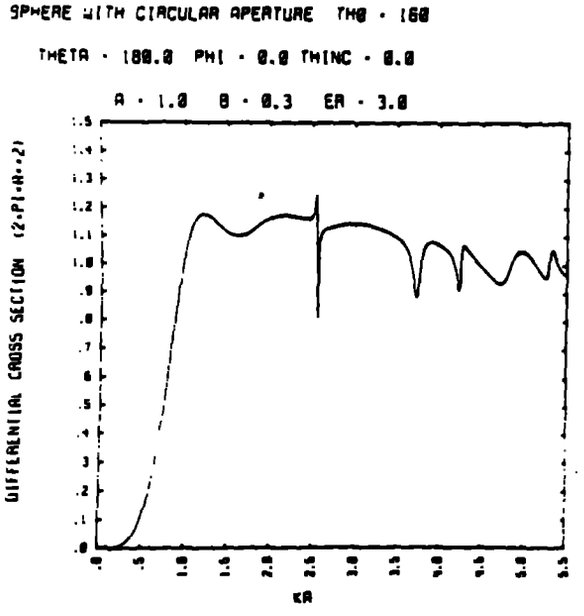
SPHERE WITH CIRCULAR APERTURE TH0 = 160
THETA = 180.0 PHI = 0.0 THINC = 0.0
A = 1.0 B = 0.3 ER = 3.0
DIFFERENTIAL CROSS SECTION (2*PI*A**2)
KA

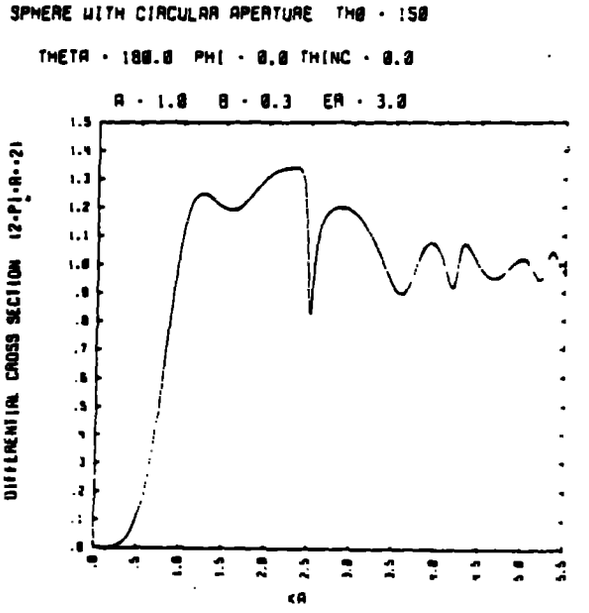
SPHERE WITH CIRCULAR APERTURE TH0 = 150
THETA = 180.0 PHI = 0.0 THINC = 0.0
A = 1.0 B = 0.3 ER = 3.0
DIFFERENTIAL CROSS SECTION (2*PI*A**2)
KA

Figure 6.

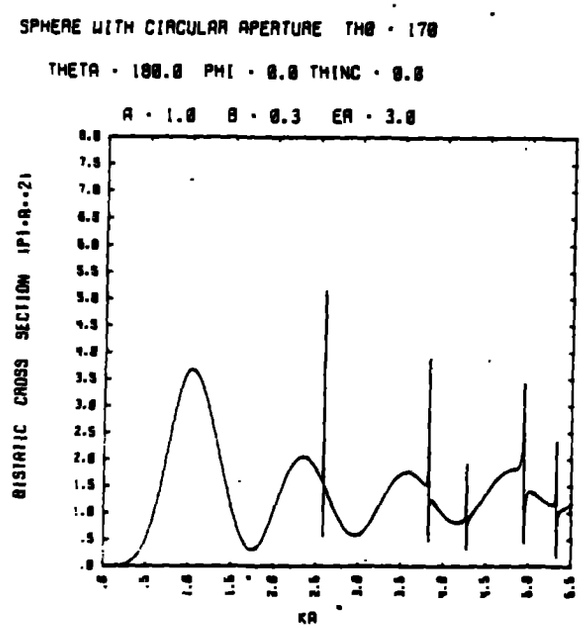
SPHERE WITH CIRCULAR APERTURE THØ = 170
THETA = 180.0 PHI = 0.0 THINC = 0.0
A = 1.0 B = 0.3 ER = 3.0
BISTATIC CROSS SECTION (PI*A**2)
KA

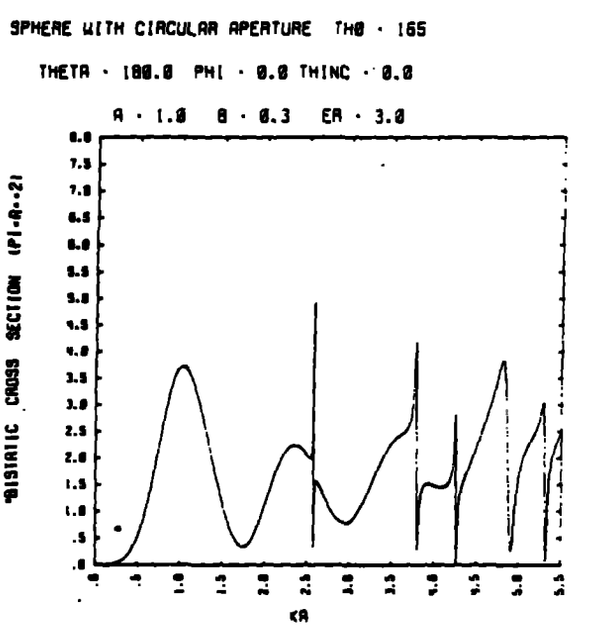
SPHERE WITH CIRCULAR APERTURE THØ = 165
THETA = 180.0 PHI = 0.0 THINC = 0.0
A = 1.0 B = 0.3 ER = 3.0
BISTATIC CROSS SECTION (PI*A**2)
KA

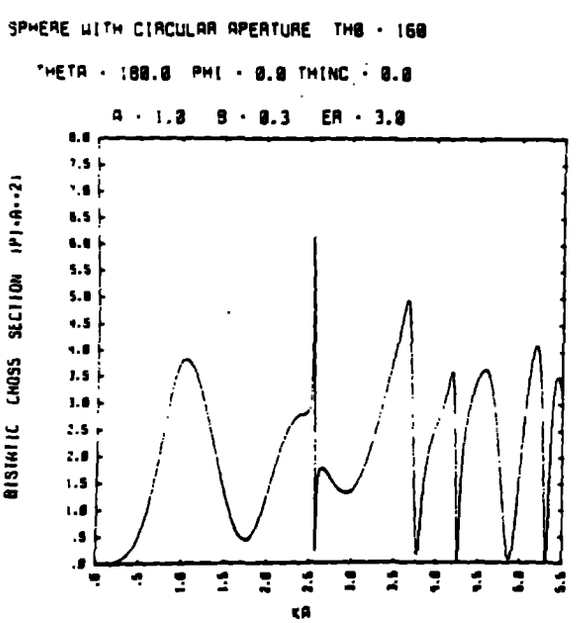
SPHERE WITH CIRCULAR APERTURE THØ = 160
THETA = 180.0 PHI = 0.0 THINC = 0.0
A = 1.0 B = 0.3 ER = 3.0
BISTATIC CROSS SECTION (PI*A**2)
KA

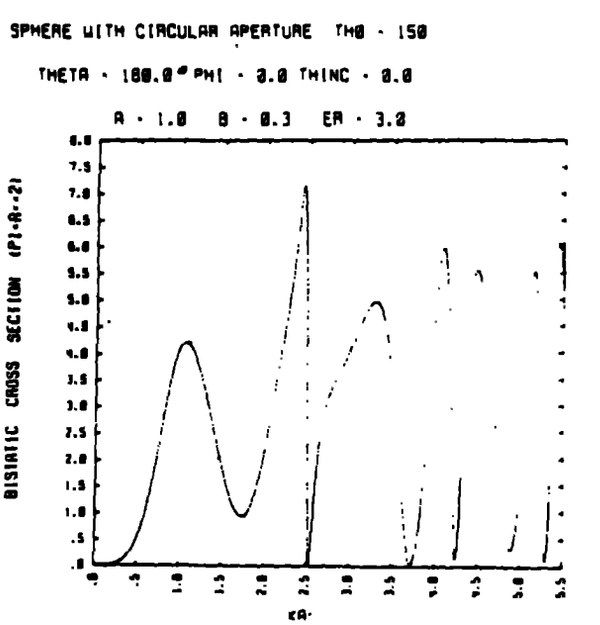
SPHERE WITH CIRCULAR APERTURE THØ = 150
THETA = 180.0 PHI = 0.0 THINC = 0.0
A = 1.0 B = 0.3 ER = 3.0
BISTATIC CROSS SECTION (PI*A**2)
KA

Figure 7.

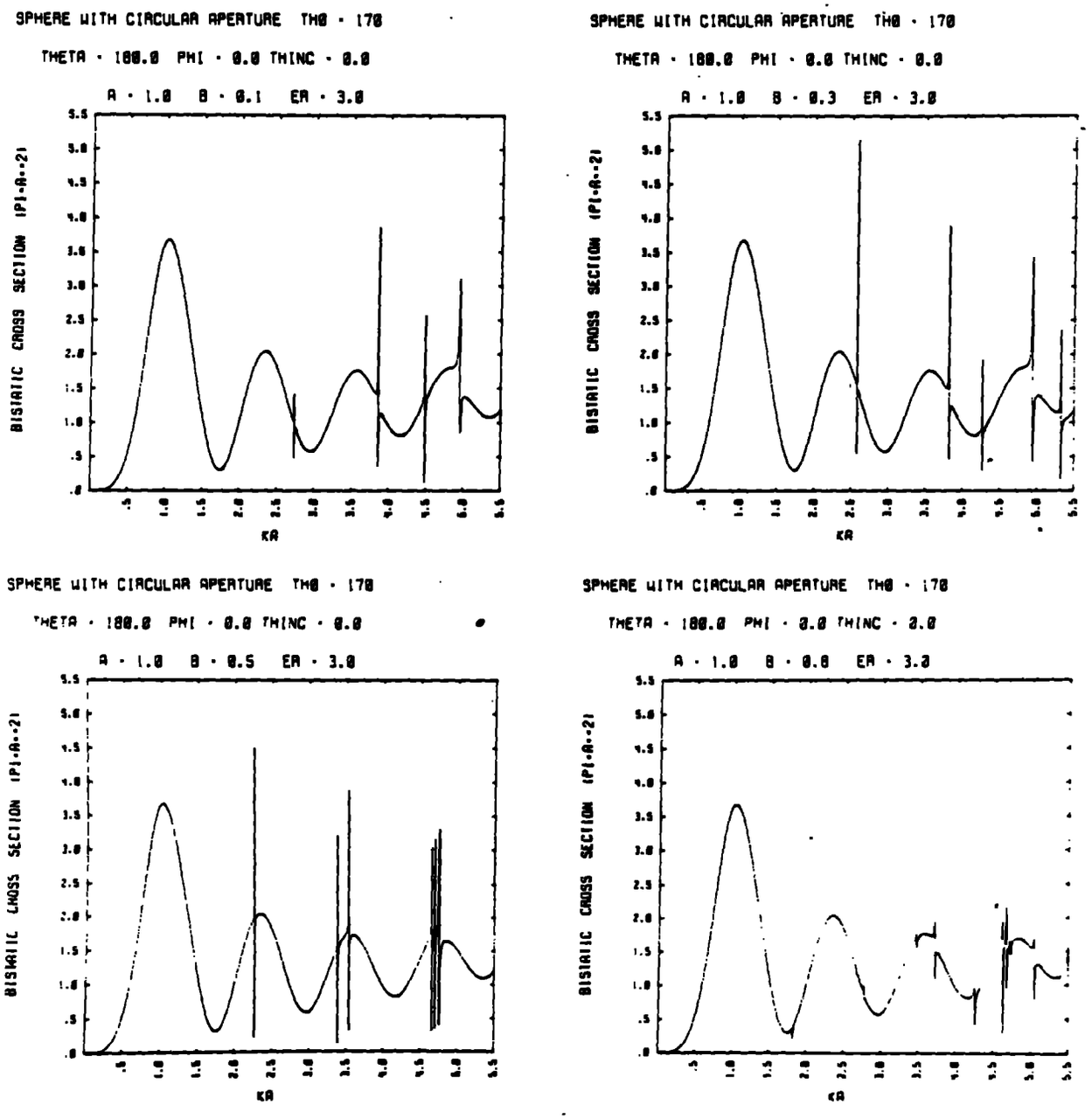
SPHERE WITH CIRCULAR APERTURE THΘ = 17Θ
THETA = 18Θ.Θ PHI = Θ.Θ THINC = Θ.Θ
A = 1.Θ B = Θ.1 ER = 3.Θ
SPHERE WITH CIRCULAR APERTURE THΘ = 17Θ
THETA = 18Θ.Θ PHI = Θ.Θ THINC = Θ.Θ
A = 1.Θ B = Θ.3 ER = 3.Θ
SPHERE WITH CIRCULAR APERTURE THΘ = 17Θ
THETA = 18Θ.Θ PHI = Θ.Θ THINC = Θ.Θ
A = 1.Θ B = Θ.5 ER = 3.Θ
SPHERE WITH CIRCULAR APERTURE THΘ = 17Θ
THETA = 18Θ.Θ PHI = Θ.Θ THINC = Θ.Θ
A = 1.Θ B = Θ.8 ER = 3.Θ
BISTATIC CROSS SECTION (PI-A--2)
KA

Figure 8.

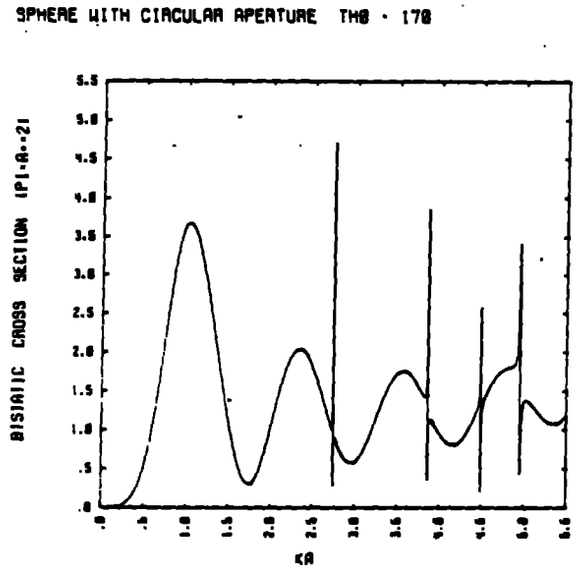
SPHERE WITH CIRCULAR APERTURE TH0 = 170
BISTATIC CROSS SECTION (PI-A--2)
KA

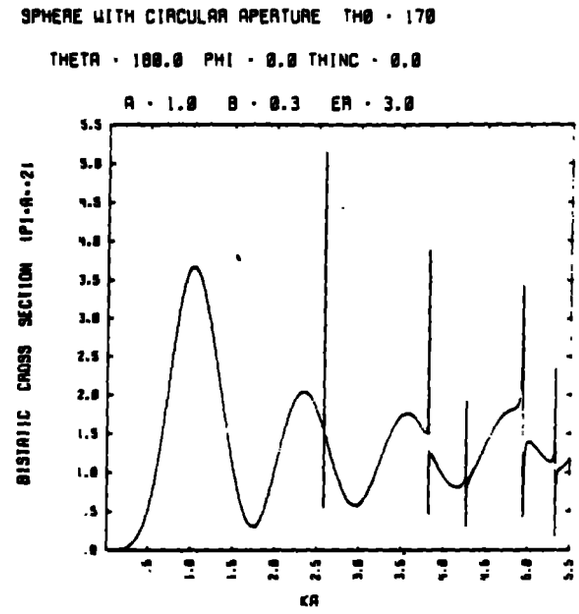
SPHERE WITH CIRCULAR APERTURE TH0 = 170
THETA = 180.0 PHI = 0.0 THINC = 0.0
A = 1.0 B = 0.3 ER = 3.0
BISTATIC CROSS SECTION (PI-A--2)
KA

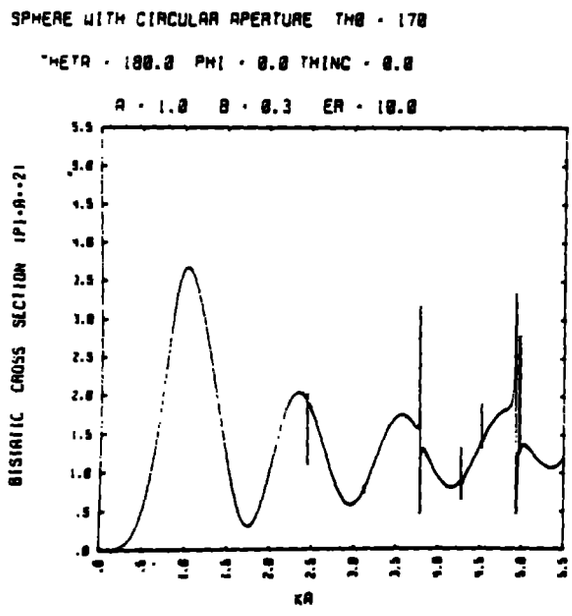
SPHERE WITH CIRCULAR APERTURE TH0 = 170
THETA = 180.0 PHI = 0.0 THINC = 0.0
A = 1.0 B = 0.3 ER = 10.0
BISTATIC CROSS SECTION (PI-A--2)
KA

Figure 9.

FIGURE 10. A COMPOSITE OF THE TE EIGENVALUES $k_{np}^{(1)}(R;\varepsilon_r = 3)a$ FOR THE SPHERICAL CAVITY OF RADIUS a FILLED WITH DIELECTRIC ε_1 INTERNALLY LOADED WITH A CONCENTRIC DIELECTRIC SPHERE OF RADIUS b AND STRENGTH $\varepsilon_2 = 3\varepsilon_1$

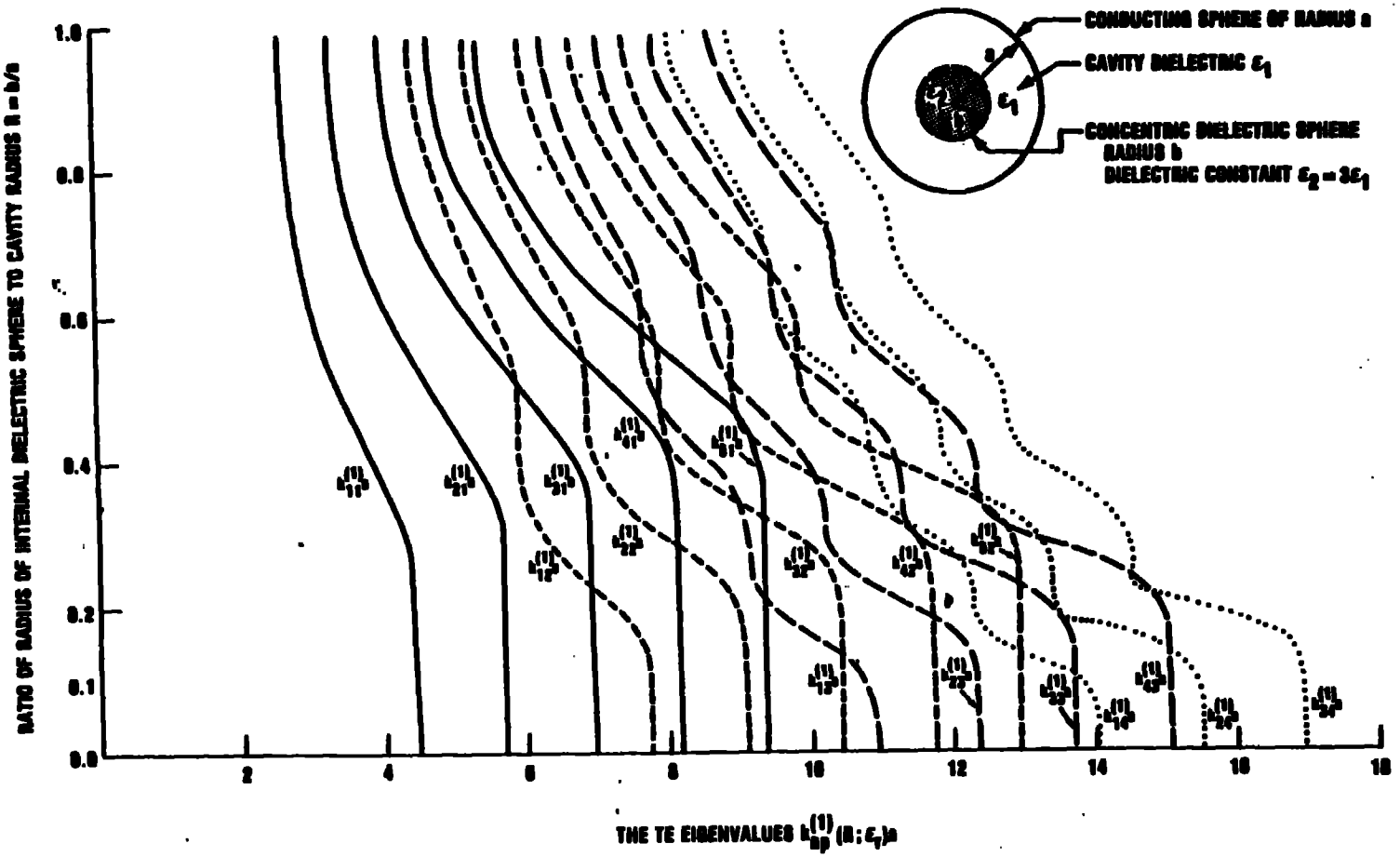

FIGURE 11. A COMPOSITE OF THE TM EIGENVALUES $k_{np}^{(2)}(R;\varepsilon_r = 3)a$ FOR THE SPHERICAL CAVITY OF RADIUS a FILLED WITH DIELECTRIC ε_1 INTERNALLY LOADED WITH A CONCENTRIC DIELECTRIC SPHERE OF RADIUS b AND STRENGTH $\varepsilon_2 = 3\varepsilon_1$